Analyst

Accepted Manuscript

This article can be cited before page numbers have been issued, to do this please use: D. Šaki and T. Weitner, *Analyst*, 2026, DOI: 10.1039/D6AN00106H.

ROYAL SOCIETY OF CHEMISTRY

rsc.li/analyst

View Article Online
DOI: 10.1039/D6AN00106H

COMMUNICATION

A Two-Point Fluorescence Detection Flow Cell with Empirical Calibration for High Optical Density Analysis

Tin Weitner[a,b] and Davor Šakić*[a,b]

Received 00th January 20xx,
Accepted 00th January 20xx

DOI: 10.1039/x0xx00000x

A two-point fluorescence detection flow cell with empirical calibration is presented for correcting inner-filter effects at high optical densities. Using only fluorescence signals from fixed detection points, linear fluorescence–concentration relationships are restored under static sample and flow conditions, demonstrating a general strategy for quantitative measurements in compact flow systems.

Fluorescence spectroscopy provides high sensitivity and selectivity for chemical analysis, yet quantitative measurements are often compromised by inner-filter effects (IFE) that distort the fluorescence–concentration relationship at moderate to high absorbances.[1,2,3] Primary attenuation of the excitation beam and secondary re-absorption of emitted light compress signal response and reduce dynamic range, often necessitating dilution or absorbance-based correction strategies. While these correction strategies can be effective in conventional cuvettes, they are generally incompatible with compact flow cells and continuous-flow measurements.[4,5,6] Consequently, a general approach that enables accurate fluorescence quantification at elevated optical densities in fixed-geometry flow channels remains of significant analytical interest.[7]

Modern efforts to address this limitation increasingly rely on mathematical and algorithmic correction strategies. Refined secondary-IFE compensation models and geometry-dependent emission corrections have extended the usable absorbance range in conventional systems.[8-11] Advances in multi-way fluorescence calibration and excitation–emission matrix (EEM) analysis, supported by dedicated computational tools, further demonstrate the shift toward data-driven extraction of quantitative information from fluorescence signals. Recent computational and multi-way calibration approaches further emphasize the need for geometry-independent, absorbance-free correction strategies.[14]

Approaches using two-position or variable-focus measurements demonstrate that position-dependent fluorescence information can be exploited for IFE correction.[8-11] However, these methods typically rely on movable optics and/or sample and are not readily transferable to flow systems.[1,6,7] We therefore hypothesized that multiple fixed fluorescence detection points within a flow cell could provide sufficient information to account for excitation and emission attenuation without requiring absorbance measurements. Building on this concept, we developed a compact multidetector fluorescence flow cell combined with a software-based calibration procedure that relates position-resolved fluorescence signals to analyte concentration. Here we present a proof-of-principle demonstration using fluorescein in strongly absorbing alkaline solution. The approach employs numerical optimization of a parametric model relating fluorescence signals from two detection points to analyte concentration, enabling calibration-based correction of inner-filter effects. Experimental validation illustrates a generalizable strategy for fluorescence measurements under high optical density conditions in flow-based systems.

Fluorescence measurements were performed using a fiber-coupled flow-cell module interfaced to an Ocean Optics S2000 spectrophotometer equipped with a Sony ILX511 CCD detector and L2 lens configuration for enhanced sensitivity (Ocean Optics, USA). The entrance slit width was 25 µm. Excitation light was provided by a PX2 xenon pulsed lamp (10 Hz, 100 ms pulse width). Emission spectra were recorded over 190–859 nm (2048 pixels) using a 3000 ms integration time, averaging ~30 lamp pulses per spectrum. No onboard smoothing or averaging was applied. Spectral acquisition was controlled using Ocean Insight software (v2.20 with OmniDriver v2.56).

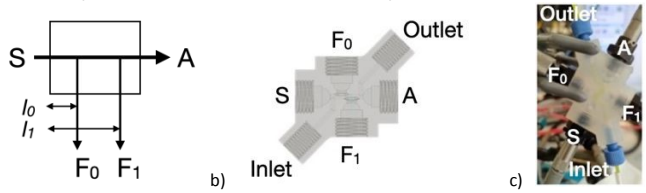

Figure 1. a) Schematic representation of the fluorescence flow cell with two fixed fluorescence detection points (F_0 and F_1), b) flow cell design, and c) assembled flow-cell module with optical and fluidic connections.

[a.] University of Zagreb Faculty of Pharmacy and Biochemistry, Ante Kovačića 1, 10000 Zagreb, Croatia
[b.] TINFE HTS llc., Havidićeva 24, 10010 Zagreb, Croatia

Raw and processed fluorescence data, instrument exports and implementation in Excel supporting this study are available from the Zenodo repository at DOI: 10.5281/zenodo.18393535

View Article Online
DOI: 10.1039/D5AN00106H

A custom-designed fluorescence flow cell was used (Figure 1). The flow-cell body was fabricated by stereolithography using Formlabs Form 3 printer and Durable Resin material (Formlabs, USA, RS-F2-DUCL-02). During all measurements, the assembled cell was externally wrapped with an opaque black polymer sheet to eliminate ambient and lateral stray light. Excitation and emission beam paths are defined by fixed quartz ball lenses mounted in the optical ports and by the CAD-defined source–detector geometry. Stray-light contributions were evaluated using lamp-off (dark) measurements and lamp-on blank measurements (buffer only). Within the emission window used for signal extraction, blank spectra did not exhibit intensity above the detector noise level, indicating that stray-light contributions are below the detectable level under the investigated conditions.

Two fluorescence detection points (F_0, F_1) were positioned along the excitation path with source (S) and absorbance detection point (A) on each end (Figure 1a). The centre-to-centre distance between F_0 (l_0 = 3.4 mm) and F_1 (l_1 = 6.4 mm) detection points was 3.0 mm. All optical ports (S, A, F_0, F_1) were equipped with 5 mm quartz ball lenses (Edmund optics, USA, 67-386) in direct contact with the liquid, sealed by o-rings and coupled to 3/8-24 collimating lens (Avantes, Netherlands, COL-UV/VIS) with SMA adapters. Optical signals were transmitted using 600 µm core solarization-resistant UV/Vis optical cable (Avantes, FC-UV600-1-SR). The assembled flow-cell module is shown in Figure 1c. In this prototype implementation, the outputs from F_0 and F_1 were acquired sequentially using a single-channel detector with time-multiplexing. This configuration may introduce systematic differences in absolute signal intensity due to optical coupling and alignment variability between the two acquisitions. However, these effects are not treated as negligible and are incorporated into the empirical calibration parameters. For potential future real-time or continuous monitoring applications, a dual-channel detection system or rapid optical switching is recommended to enable near-simultaneous acquisition.

Although the cell design includes an absorbance port (A), absorbance detection was not required for the fluorescence calibration model presented here. For the continuous-flow gradient experiments, UV absorbance at 280 nm was monitored downstream using the ÄKTA UV module solely to reconstruct the effective gradient composition delivered to the flow cell. This external absorbance measurement was used as an independent reference for gradient-axis correction and was not incorporated into the fluorescence correction algorithm.

The flow inlet and outlet ports were connected using standard 1/4-28 fittings with ferrule and 1/16” OD PTFE tubing (ID 1/32”). Three-way, 90° low pressure valves (Hamilton, USA, HVP-86778) were installed at both the inlet and outlet to enable bubble removal, bidirectional flushing, and liquid isolation during acquisition. The internal cell volume was <100 µL, with ~500 µL of connecting tubing. Bubble removal was verified optically by monitoring a stable lamp signal while briefly flowing liquid in both directions; the absence of transient intensity fluctuations indicated a bubble-free optical path.

The performance of the fluorescence flow cell was evaluated under two distinct operating modes. Under static sample conditions, individual samples were manually loaded, measured, and flushed between acquisitions. Under continuous-flow gradient conditions, fluorescence was recorded during on-line concentration changes under steady flow. In addition to the coefficient of determination (R^2), two dimensionless metrics were used to characterize method performance under strong inner-filter effects: the limit of detection as a percentage of the maximum tested concentration (LOD%) and the percent error in the slope of the corrected signal (mErr%). LOD% quantifies sensitivity, while mErr% reflects the deviation from ideal linearity in the calibration fit.[1] Together, these metrics provide scale-independent assessment of quantification accuracy across different analytes or concentration ranges.

For static sample conditions, fluorescein (FL) standards were prepared in 0.1 M NaOH from a stock solution (c = 5.88 × 10^{-4} M), verified spectrophotometrically (ε_{490} = 87 100 M^{-1} cm^{-1}).[5,15] A 2:1 serial dilution series of FL was generated over the concentration range of approximately 1-40 µM (7 points). At the highest concentration, the absorbance at the excitation wavelength reached $A_{490} \approx 3.2$ when normalized to a 1 cm optical path, resulting in pronounced IFE (see Figure 2). For each concentration, lamp-off (dark) and lamp-on spectra were acquired with the cell hydraulically locked using the 3-way valves. Spectra were independently processed using a Savitzky–Golay (SG) convolution (21-point window, 3rd-order polynomial).[16]

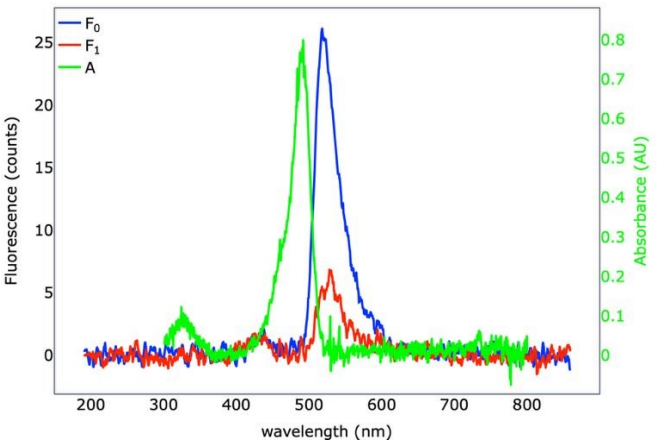

Figure 2. Raw fluorescence emission spectra acquired at detection points F_0 and F_1 (left y-axis) for c(Fluorescein) = 3.68 × 10^{-5} M in 0.1 M NaOH. Absorbance spectrum at detection point A (l = 9.8 mm, right y-axis) was measured for c(Fluorescein) = 9.19 × 10^{-6} M in 0.1 M NaOH.

Because SG filtering and dark subtraction are linear operations, their order is interchangeable within the retained pixel range. Dark-corrected, SG-filtered emission spectra were computed as the difference between the smoothed lamp-on and lamp-off spectra (Figure 2).

Fluorescence signals F_0 and F_1 were extracted by integrating a 10 nm window (± 5 nm) centred at λ = 517 nm (~24 CCD pixels), corresponding to the emission maximum observed at both detection points. As analyte concentration increased, both

View Article Online
DOI: 10.1039/D6AN00106H

signals exhibited pronounced attenuation due to inner-filter effects. At higher absorbances, the proximal detector (F_0) showed nonlinear signal compression, while the distal detector (F_1) approached the detector noise floor, consistent with strong attenuation of excitation and emission along the optical path. The distinct attenuation behaviour of the two spatially separated signals provides complementary information that can be exploited for calibration-based correction of inner-filter effects.

Calibration was performed using a numerical optimization procedure inspired by the NINFE framework,[1] adapted and generalized for a dual-pathlength flow cell. A general relationship between any number of fluorescence signals and concentration is modeled according to eq1:

$$\min_{\{q_i\},\{p_d\}} \sum_{j=0}^{M} \left[\prod_{i=0}^{N} F_{i,j}{}^{-q_i} - f_j(p_0, p_1, \ldots, p_D; c_j) \right]^2$$

where c_j are concentrations used for the calibration, $\{q_0, q_1, \ldots, q_N; p_0, p_1, \ldots, p_D\}$ is the set of calibration parameters for which the smooth function $f_j(p_0, p_1, \ldots, p_D; c_j)$ is optimized by least-squares minimization. When a linear model $f = p_0 + p_1 \cdot c_j$ is selected, the calibrated relationship provides an analytic expression linking the combined fluorescence signal to concentration $c_{IFER} = (\prod_{i=0}^{N} F_i{}^{-q_i} - p_0)/p_1$.

For the present flow cell with two fluorescence detection points F_0 and F_1 ($N = 1$ and $D = 1$), the general equation eq1 reduces to eq2:

$$\min_{\{q_1,p_0,p_1\},} \sum_{j=0}^{M} \left[F_{0,j}{}^{1+q_1} \cdot F_{1,j}{}^{-q_1} - (p_0 + p_1 \cdot c_j) \right]^2$$

with only 3 calculated parameters, $\{q_1, p_0, p_1\}$ using the relationship $q_0 = -(1 + q_1)$ established in previous work.[1]

In contrast to polynomial fitting, which provides a purely descriptive curve for a given dataset, the present model combines signals measured at defined spatial positions along the excitation path. The empirical exponent captures position-dependent attenuation effects, allowing the corrected signal to reflect the underlying attenuation geometry. Within a defined absorbance range and measurement configuration, the calibrated model retained the same functional form and did not require dataset-specific modification.

Numerical optimization was performed using Solver tool in Microsoft Excel, yielding an empirical exponent q_1 = 3.021. Using a linear concentration model for the smooth function, $F_{IFE\_CORR} = p_0 + c * p_1$, with parameters $p_0 = -10.1$ and $p_1 = 15354$, linear correlation produced $R^2 > 0.99812$ across the full dilution series (Figure 3).

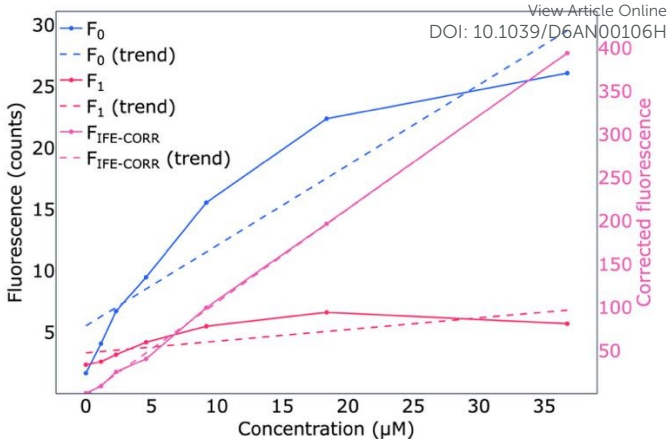

Figure 3. Fluorescence signals, F_0 and F_1, (left y-axis) and the calibrated fluorescence signal F_{IFE_CORR} (right y-axis) as a function of fluorescein concentration under static (manual) sample loading. Dashed lines indicate linear trend fits for each signal ($R^2(F_0)$ = 0.8616, $R^2(F_1)$ = 0.5643, $R^2(F_{IFE\_CORR})$ = 0.9981).

Under static sample conditions, linearity was preserved across the full absorbance range examined up to 36.8 µM, corresponding to $A_{490} \approx 3.2$ normalized to a 1 cm optical path. Within this regime, the limit of detection normalized to the maximum analyte concentration was LOD% = 5.65, and the percent error of the slope of the corrected fluorescence signal was mErr% = 0.49, indicating high quantitative accuracy.[1] This calibration demonstrates a proof-of-principle implementation of the multidetector model described in the associated patent submission.[17]

To evaluate flow performance, experiments were conducted under continuous-flow gradient conditions. A continuous fluorescein concentration gradient was generated using an ÄKTA start FPLC system (Cytiva, USA) operated without fractionation. Buffer A was 0.1 M NaOH and buffer B was a fluorescein stock solution in 0.1 M NaOH adjusted to $A_{490} \approx 5$, normalized to a 1 cm optical path, prepared from previous stock by tenfold dilution. Prior to gradient initiation, the fluorescence flow cell was thoroughly rinsed with approximately 10 mL of buffer A to avoid sample carryover between gradient runs. A linear 0–100% B gradient was programmed over 10 mL at a constant flow rate of 1.0 mL min^{-1} using the instrument's built-in static mixer (V = 0.4 mL). The effective gradient profile was reconstructed from UV absorbance to account for system dispersion and delay volume. The gradient enabled gradual on-line mixing of fluorescein during flow through the cell; no fractions were collected.

To verify and correct the actual gradient profile delivered to the flow cell, UV absorbance at 280 nm was monitored on-line during the same run using the ÄKTA UV detector (optical path length 0.2 cm). The maximum observed absorbance was approximately $A_{280} \approx 145$ mAU, corresponding to $A_{490} \approx 4.5$, normalized to 1 cm optical path. This value was extrapolated by using the ratio of molar extinction coefficients at 490 nm and 280 nm (ε_{490} = 87 100 M^{-1} cm^{-1} and ε_{280} = 15 240 M^{-1} cm^{-1}) and corresponding pathlengths (l_{490} = 1 cm and l_{280} = 0.2 cm). The recorded A_{280} trace was used as an independent proxy for the effective %B composition and revealed the expected non-

View Article Online
DOI: 10.1039/D5AN00106H

linearity at the beginning and end of the programmed gradient due to valve duty-cycle limits and mixer dispersion. Consequently, only the central 2–98% B region of the gradient was used for inner-filter effect analysis, while the initial and final 2% were excluded. This measured UV profile was therefore used to generate a corrected gradient axis for subsequent data analysis, in which the recorded signal was mapped onto an ideal linear gradient.

Fluorescence measurements under flow conditions were performed using the same optical setup as in the static sample experiment, except that 1000 µm core UV/IR optical cables (Avantes, FC-UV1000-1) were used to increase signal sensitivity. Because a single-channel spectrometer was employed, two separate gradient runs were performed to collect fluorescence signals F_0 and F_1. A total of 64 time points were recorded up to the concentration of 48 µM (Figure 4). In contrast to the static sample experiments, raw baseline-corrected data were used, where the baseline was defined as the average of 20 data points collected prior to gradient initiation under lamp-on conditions in the absence of fluorescein. The 3000 ms integration time of the spectrophotometer corresponds to < 0.4 % of total gradient duration and therefore does not introduce significant concentration averaging error.

Applying the same calibration procedure as described above, the empirical exponent in eq2 was optimized to $q_1 = 1.310$. The resulting calibrated signal exhibited strong linearity, with $R^2 >$ 0.99750, and parameters $p_0 = 15.6$ and $p_1 = 66467$. Linearity was maintained over the central portion of the gradient, corresponding to a 1 cm-normalized absorbance range of approximately $A_{490} = 0.09–4.18$. Within this range, the limit of detection expressed as a percentage of the highest analyte concentration in the series was LOD% = 6.26, where LOD values were normalized to the maximum concentration of the corresponding dataset. The percent error of the slope of the corrected fluorescence signal was mErr% = 2.15, indicating good quantitative stability of the calibrated response under flow conditions.

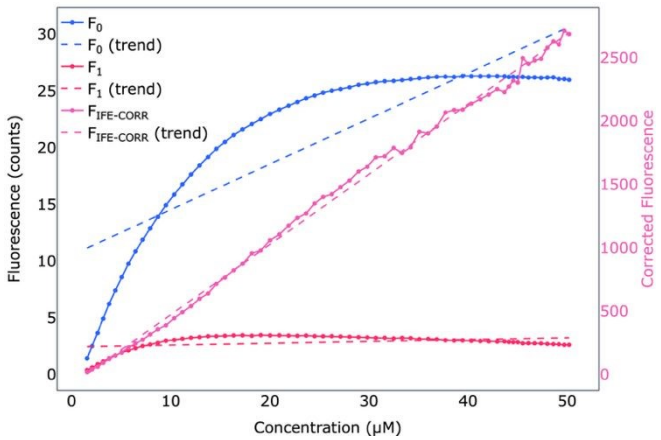

Figure 4. Fluorescence signals, F0 and F1, (left y-axis) and the calibrated fluorescence signal F_{IFE_CORR} (right y-axis) as a function of fluorescein concentration under continuous gradient flow conditions. Dashed lines indicate linear trend fits for each signal ($R^2(F_0) = 0.7195$, $R^2(F_1) = 0.0071$, $R^2(F_{IFE\_CORR}) = 0.9967$).

If concentration-dependent quenching were significant within the investigated concentration range (up to 50 µM), a systematic deviation from linearity would remain after correction of optical attenuation. No such residual curvature or slope compression was observed. This suggests that, under the present conditions and concentration range, signal distortion is dominated by optical attenuation (primary and secondary inner-filter effects), while any contribution from self-quenching is below the detectable level.

The apparent discrepancy between the raw and corrected fluorescence scales in the two datasets requires clarification. While the raw F_0 signals were of similar magnitude in the experiments shown in Figures 3 and 4, the corrected fluorescence is not a directly measured intensity, but a derived quantity obtained from a nonlinear combination of F_0 and F_1. Its absolute magnitude therefore depends not only on the measured channel intensities, but also on their relative scaling and on the optimized empirical exponent q_1. Because these parameters differed between the two independently calibrated experiments, the absolute values of the corrected signals are not expected to match directly, even when the raw F_0 traces appear similar. This is because the distal signal (F_1) is generally more strongly affected by attenuation and alignment sensitivity than the proximal signal (F_0), making it more susceptible to variations in optical coupling and experimental configuration. The relevant outcome is therefore not the absolute corrected signal level itself, but the restoration of a linear concentration response within each experimental configuration.

Differences in optimized q_1 between static and flow experiments likely reflect the different calibration regimes rather than a change in any single underlying physical parameter. In the static measurements, discrete standards were measured under stationary conditions with directly defined concentrations. In the flow experiments, by contrast, calibration was performed during a continuous gradient, with concentration assigned indirectly from the UV/gradient reference and with the fluorescence signals subject to transport, dispersion, and signal-alignment effects (sequential acquisition of F_0 and F_1 signals). These factors may introduce additional sources of variability that can influence the optimized empirical parameters and thereby alter the scale of the corrected response. Accordingly, absolute fluorescence intensities are not directly comparable between independent, separately calibrated experiments, because they are influenced by optical coupling, fibre alignment, detector scaling, and acquisition mode. Interpretation is therefore based on the relative signal behaviour and on the resulting calibrated concentration response within each experiment.

To assess the influence of hydrodynamic conditions on the calibration, an additional experiment was performed at a reduced flow rate of 0.5 mL min^{-1} (see Zenodo repository for details). The corrected fluorescence signal retained excellent linearity ($R^2 >$ 0.99750), comparable to that obtained at 1.0 mL min^{-1}, with similar LOD and slope error metrics. This indicates that the calibration remains effective under moderate changes in flow rate and residence time for the present system.

View Article Online
DOI: 10.1039/D5AN00406H

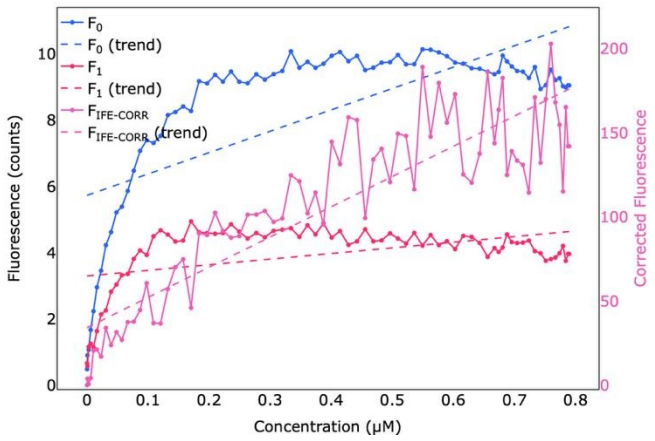

Figure 5. Fluorescence signals, F_0 and F_1, (left y-axis) and the calibrated fluorescence signal F_{IFE_CORR} (right y-axis) as a function of quinine sulfate concentration under continuous gradient flow conditions. Dashed lines indicate linear trend fits for each signal ($R^2(F_0)$ = 0.7070, $R^2(F_1)$ = 0.5065, $R^2(F_{IFE\_CORR})$ = 0.8652).

However, the raw fluorescence signals were flow-rate dependent, indicating that the relationship between the programmed gradient and the measured detector response is shaped by both optical effects and flow-dependent transport processes.

These effects are reflected in the optimized calibration parameters, which differed between flow conditions. More generally, the calibration parameters are both flow-dependent and analyte-dependent and should therefore be determined empirically for each measurement configuration.

Although the present study focuses on fluorescein as a model analyte, the proposed correction framework is not restricted to a specific emission spectrum or Stokes shift. Because the calibration is empirical and based on position-resolved attenuation rather than explicit spectral overlap assumptions, adaptation to other fluorophores is achieved through compound-specific calibration. Complementary experiments with quinine sulfate (Figure 5), which exhibits a larger Stokes shift and reduced emission reabsorption, further demonstrate the general applicability of the approach across different attenuation regimes. In this case, the corrected signal exhibited weaker calibration performance with reduced linearity (R^2 > 0.86524) and reduced sensitivity (LOD% = 41.8), primarily due to lower fluorescence intensity and increased noise in the raw signals. Because the calibration model combines signals multiplicatively, noise present in F_0 and F_1 is amplified. Despite this limitation, the slope error remained moderate (mErr% ≈ −6.9%), indicating that the underlying model structure remains valid. These results suggest that performance in low-emission systems is primarily limited by instrumental sensitivity rather than by the calibration approach itself.

In conclusion, inner filter effects limit the dynamic range of fluorescence measurements, restricting their applicability for quantitative analysis at elevated analyte concentrations. Here we introduce a compact fluorescence flow cell (< 100 µL cavity) incorporating two fixed fluorescence detection points along the excitation axis, together with a numerical calibration that relies exclusively on fluorescence signals. The method fits a smooth parametric model describing the position-dependent fluorescence response and enables calibration-based correction of inner filter effects under both static and flow conditions.

The system requires no movable optics or absorbance measurements and is compatible with continuous-flow operation. Classical geometric cell-shift models assume a uniform excitation beam path and a symmetric fluorescence observation field within the cell.[7] In practice, real flow cells deviate from these assumptions due to optical effects. An empirically calibrated model can implicitly account for these effects, yielding a much more robust linear fluorescence–concentration relationship.

Using fluorescein as a model analyte, the flow cell approach achieved linearity for absorbance up to A_{490} ≈ 3.2, normalized to a 1 cm optical path (R^2 > 0.99812). The continuous flow-gradient experiment demonstrated high stability and reproducibility in multiple runs, maintaining strong linearity (R^2 > 0.99669) for absorbance up to A_{490} ≈ 4.2, normalized to a 1 cm optical path. Static experiments validate geometric correction under equilibrium conditions, while flow experiments assess robustness under dynamic concentration gradients relevant to process monitoring. For quinine sulfate, linearization was achieved up to A_{345} ≈ 3.6, normalized to a 1 cm optical path, with reduced but still meaningful correlation (R^2 > 0.86524). The lower linearity and higher detection limits observed in this case are attributed primarily to reduced fluorescence intensity and increased noise propagation in the correction model, rather than a breakdown of the underlying attenuation-based calibration principle.

Together, these results demonstrate a generalizable framework for quantitative fluorescence analysis under conditions of high optical density. While the presented flow cell and calibration model were developed using fluorescein as a model compound, the approach based on two-point fluorescence detection and empirical calibration can be adapted to other fluorophores or sample matrices through compound-specific calibration.

Author contributions

TW: methodology, investigation, validation, data curation, writing – review and editing. DŠ: formal analysis, visualization, software, writing – original draft.

Conflicts of interest

Davor Šakić and Tin Weitner are co-founders of the TINFE HTS LLC, Croatia, and have jointly developed flow cell used herein, as well as TINFE program package for data processing, analysis, processing, and reporting. Both products are commercial, and under patent application submitted to the EPO office with application No. EP25220873.1, filed on December 4th, 2025.

Data availability

View Article Online
DOI: 10.1039/D6AN00106H

Raw and processed fluorescence data, instrument exports and implementation in Excel supporting this study are available from the Zenodo repository at DOI: 10.5281/zenodo.18393535.

Notes and references

1 T. Weitner, T. Friganović and D. Šakić, *Anal. Chem.*, 2022, **94**, 7107–7114, DOI: **10.1021/acs.analchem.2c01031**.
2 S. K. Panigrahi and A. K. Mishra, *J. Photochem. Photobiol. C: Photochem. Rev.*, 2019, **41**, 100318, DOI: **10.1016/j.jphotochemrev.2019.100318**.
3 M. Kubista, R. Sjöback, S. Eriksson and B. Albinsson, *Analyst*, 1994, **119**, 417–419, DOI: **10.1039/AN9941900417**.
4 N. K. Subbarao and R. C. MacDonald, *Analyst*, 1993, **118**, 913–916, DOI: **10.1039/AN9931800913**.
5 J. N. Miller, in *Standards in Fluorescence Spectrometry (Techniques in Visible and Ultraviolet Spectrometry)*, Springer, Dordrecht, 1981, pp. 27–43, DOI: **10.1007/978-94-009-5902-6_5**.
6 NanoTemper Technologies GmbH, *EU Pat.*, EP 4328569 A1, 2022. "Method and apparatus for measuring high protein concentrations".
7 H.-P. Lutz and P.L. Luisi, *Helvetica Chimica Acta,* 1983, **66**(7), 1929–1935, DOI: **10.1002/hlca.19830660704**
8 W. Li, Y. Fu, T. Liu, H. Li and M. Huang, *Spectrochim. Acta Part A: Mol. Biomol. Spectrosc.*, 2023, **288**, 122147, DOI: **10.1016/j.saa.2022.122147**
9 X. Li, Z. Zhou, T. Yang, J. Qiang and X. Wang, *Measurement,* 2025, **256**, 118467, DOI: **10.1016/j.measurement.2025.118467**
10 Z. Liu, Y. Bi, W. Chu, W. Li and P. Wang, *IEEE Trans. Instrum. Meas*., 2025, **74**, 1–7, DOI: **10.1109/TIM.2025.3556817**
11 L. Brack, O. Merkel and R. Schroeder**, *Eur. J. Pharm. Biopharm.,*** 2024, **201**, 114377, DOI: **10.1016/j.ejpb.2024.114377**
12 M. Antonio, A. Muñoz de la Peña, H. C. Goicoechea and M. R. Alcaraz, *Anal. Chim. Acta*, 2025, **1360**, 344089, DOI: **10.1016/j.aca.2025.344089**
13 D. Omanović, S. Marcinek and C. Santinelli, *Water*, 2023, **15**, 2214, DOI: **10.3390/w15122214**
14 L. Zhou, Y. Chen, S. Yang, Y. Li and N. Dai, *Microchem. J.*, 2026, **182**, 117390, DOI: **10.1016/j.microc.2026.117390**
15 P. C. DeRose and G. W. Kramer, *Journal of Luminescence*, 2005, **113**, 314–320, DOI: **10.1016/j.jlumin.2004.11.002**
16 A. Savitzky and M. J. E. Golay, *Anal. Chem.*, 1964, **36**, 1627–1639, DOI: **10.1021/ac60214a047**.
17 TINFE HTS LLC, *EU Pat.*, EP 25220873.1, 2025.

View Article Online
DOI: 10.1039/D6AN00106H

Davor Šakić, PhD

University of Zagreb
Faculty of Pharmacy and Biochemistry
Ante Kovačića 1, 10000 Zagreb, Croatia

and

TINFE HTS LLC
Havidićeva 24, 10010 Zagreb, Croatia

E-mail: davor.sakic@pharma.unizg.hr, davor@tinfe.tech
Phone: +385 91 561 7246

Zagreb, January 28th, 2026

Data availability

The data supporting the findings of this study, including raw and processed fluorescence spectra, calibration datasets, continuous-flow gradient metadata, and exported raw instrument files, are openly available in the Zenodo repository at https://doi.org/10.5281/zenodo.18393535.

Sincerely

Davor Šakić, PhD